Received: 30 May 2016 | Revised: 22 November 2016 | Accepted: 22 November 2016

DOI: 10.1002/nbm.3687

WILEY NMR IN BIOMEDICINE

RESEARCH ARTICLE

On the transmit field inhomogeneity correction of relaxation-compensated amide and NOE CEST effects at 7 T

Vitaliy Khlebnikov[1] | Johannes Windschuh[2] | Jeroen C.W. Siero[1,3] | Moritz Zaiss[2] | Peter R. Luijten[1] | Dennis W.J. Klomp[1] | Hans Hoogduin[1]

[1] Department of Radiology, University Medical Center Utrecht, Utrecht, The Netherlands

[2] Division of Medical Physics in Radiology, Deutsches Krebsforschungszentrum (DKFZ) [German Cancer Research Center], Heidelberg, Germany

[3] Spinoza Centre for Neuroimaging, Amsterdam, The Netherlands

Correspondence
Vitaliy Khlebnikov, Department of Radiology, University Medical Center Utrecht, Utrecht, The Netherlands.
Email: v.khlebnikov@umcutrecht.nl

High field MRI is beneficial for chemical exchange saturation transfer (CEST) in terms of high SNR, CNR, and chemical shift dispersion. These advantages may, however, be counter-balanced by the increased transmit field inhomogeneity normally associated with high field MRI. The relatively high sensitivity of the CEST contrast to B_1 inhomogeneity necessitates the development of correction methods, which is essential for the clinical translation of CEST. In this work, two B_1 correction algorithms for the most studied CEST effects, amide-CEST and nuclear Overhauser enhancement (NOE), were analyzed. Both methods rely on fitting the multi-pool Bloch-McConnell equations to the densely sampled CEST spectra. In the first method, the correction is achieved by using a linear B_1 correction of the calculated amide and NOE CEST effects. The second method uses the Bloch-McConnell fit parameters and the desired B_1 amplitude to recalculate the CEST spectra, followed by the calculation of B_1-corrected amide and NOE CEST effects. Both algorithms were systematically studied in Bloch-McConnell equations and in human data, and compared with the earlier proposed ideal interpolation-based B_1 correction method. In the low B_1 regime of 0.15–0.50 μT (average power), a simple linear model was sufficient to mitigate B_1 inhomogeneity effects on a par with the interpolation B_1 correction, as demonstrated by a reduced correlation of the CEST contrast with B_1 in both the simulations and the experiments.

KEYWORDS

B_1 correction, Bloch-McConnell equations, relaxation-compensated amide-CEST, relaxation-compensated NOE CEST, transmit field inhomogeneity

1 | INTRODUCTION

Chemical exchange saturation transfer (CEST) is a magnetization transfer (MT)-based contrast allowing the low concentration metabolite pools bearing exchangeable protons to be detected indirectly through the abundant exchange-mediating water proton pool.[1–4] The water signal attenuation, originating from the saturation transfer of the irradiated protons of interest by chemical exchange to the water protons, is detected via the CEST spectrum (also known as a *Z*-spectrum).

The CEST technique in high field MRI (HF-MRI) has generated much interest in the imaging of metabolites.[5–9] Two of the most studied CEST effects are amide-CEST[10–12] and the relayed nuclear Overhauser enhancement (NOE).[13,14] Amide-CEST, which is believed to originate from the cytosolic amide metabolites, has found its application in glioma grading,[15–17] cancer therapy monitoring,[18,19] and differentiation between necrosis and tumor regrowth.[20] NOE originates from aliphatic and olefinic protons of the cellular mobile macromolecule effect and has been reported to be linked to tissue cellularity[21] and cellular membrane fluidity.[22]

The CEST contrast is unique in providing quantitative metabolite-specific information. To accurately resolve physiological spatial variations in the CEST contrast it is crucial to minimize contrast variations due to system imperfections. While CEST at HF-MRI benefits from high SNR, CNR, and chemical shift dispersion, it suffers from the consequent increased transmit field inhomogeneity. The relatively high sensitivity of the CEST contrast to B_1 inhomogeneity necessitates the development of correction methods, which is essential for the clinical translation of CEST. Previously, Windschuh et al. proposed an

interpolation-based approach to correct *Z*-spectra and CEST contrast for B_1 inhomogeneity.[23] In this approach, the densely sampled *Z*-spectra are acquired at at least two different B_1 levels, and B_1 correction of *Z*-spectra and isolated CEST contrast is achieved by spline interpolation of the multiple B_1 data to a B_1 of interest. However, this approach may not be possible in a clinical setting, where the scan time is very limited.

In this work, two methods that require only one CEST dataset at a particular B_1 level and a relative B_1 map as a reference are compared. Both methods rely on fitting the multi-pool Bloch-McConnell equations[24] to the densely sampled *Z*-spectra using a B_1 map as a reference. In the first method, an assumption is made about a linear relationship of CEST effects with B_1. The B_1 correction is achieved by using a linear B_1 correction of the calculated amide and NOE CEST effects. The second method is based on an assumption that the Bloch-McConnell estimated fit parameters other than B_1 are independent of the actual B_1. The estimated fit parameters and the desired B_1 amplitude are used to recalculate the *Z*-spectra followed by the calculation of B_1-corrected amide and NOE CEST effects. Both approaches were first evaluated in simulated data and subsequently tested in data from healthy human brain.

2 | METHODS

2.1 | Generation of simulated CEST spectra

Four-pool (water, amide-CEST, NOE and MT) Bloch-McConnell equations were solved numerically[25] assuming the following white matter (WM) pool parameters[26]: (i) water (T_1/T_2 = 1.2 s/40 ms); (ii) amide-CEST (T_1/T_2 = 1 s/10 ms, exchange rate 50 Hz, pool size ratio 0.13%, chemical shift 3.5 ppm); (iii) NOE (T_1/T_2 = 1 s/0.3 ms, pool size ratio 6%, exchange rate 10 Hz, chemical shift −3.5 ppm); and (iv) MT (T_1/T_2 = 1 s/10 μs, pool size ratio 11%, exchange rate 50 Hz, chemical shift −2.4 ppm). Even though the NOE effect (−3.5 ppm) was shown to be composed of multiple fine structures,[13] we chose to approximate it with the single offset due to the use of short pulses with high bandwidth in this work. Due to large insensitivity of simulations to T_1 values of other than water pools, the T_1 of amide-CEST, NOE and MT was fixed to 1 s, as suggested previously.[27] The sequence parameters used in the simulations are the same as in the data acquisition (see later), except for the B_1 level extended up to 1.8 μT (average power). The simulations were based on the assumption that there are only four pools in the system and that the only interactions are with water.

2.2 | Data acquisition

In this report, we made a retrospective analysis of the data in Reference [23]. *In vivo* experiments were performed on a 7 T MR whole-body system (Magnetom; Siemens, Erlangen, Germany) using a Tx/Rx head coil (Tx, one channel; Rx, 24 channels). The CEST protocol was as follows[28]: saturation consisted of a train of 120, 15 ms Gaussian pulses interleaved with a GR-spoiler, duty cycle 60%; for readout a single-shot 2D gradient echo sequence (GRE) was used with GRAPPA acceleration factor 2, T_R/T_E/FA = 7.4 ms/3.6 ms/10°, matrix 128 × 128, slice thickness 5 mm. Total scan time was 4 min 7 s. *Z*-spectra were sampled at 66 frequency offsets distributed unevenly between ±500 ppm (500 ppm offset was used for normalization). The CEST sequence was performed at eight different B_1 levels: 0.14, 0.29, 0.43, 0.50, 0.58, 0.65, 0.72, and 0.80 μT. B_1 level refers to the nominally set, average power of the saturation pulse throughout the paper. B_0 inhomogeneity was corrected using the WASSR method.[29] A 2D flip-angle map was based on a single-shot GRE sequence: a rectangular preparation pulse (2 ms) with nominal flip angle 90°, T_E/T_R = 2.42 ms/5000 ms. The transmitter voltage and thus the nominal B_1 values were calibrated on the basis of this flip angle map. A relative map of irradiation amplitude ($rB_1(x, y)$) was produced by the normalization of this flip-angle map by the nominal flip angle. The actual irradiation amplitude B_1 in each pixel (x, y) was assigned employing the relative B_1 map $rB_1(x, y)$ by $B1(x, y) = rB1(x, y)B1$, nom, where $B_{1,\mathrm{nom}}$ is the nominal B_1 value as chosen in the protocol settings. A T_1-weighted anatomical image was used to produce white matter (WM) and grey matter (GM) masks in FSL (FMRIB v6.0, UK).

2.3 | Fitting Bloch-McConnell equations to the data

The four (water, amide-CEST, NOE and MT) and six (water, amide-CEST, NOE, MT, amine-CEST[23] and NOE*[22]) pool Bloch-McConnell equations were used to fit the simulated and the *in vivo Z*-spectra, respectively. The data was fitted at a single B_1 level at any given time. Since the saturation duration in the employed sequence is less than water T_1, the saturation duration was taken into account in data fitting.[25] The choice of six pools to fit the *in vivo Z*-spectra was based on the results of fitting a few test *Z*-spectra by incrementing the number of pools and monitoring the goodness-of-fit statistics. Increasing the number of pools from four to six reduced the sum of squared errors by 50% (*F*-test, $p < 0.01$). The fitting was done employing a non-linear least squares constrained optimization algorithm (lsqcurvefit function in MATLAB) and using the pool parameters[26,30–33] in Table 1. The goodness of fit was examined using Curve Fitting Toolbox™ in MATLAB with the following metrics: (i) the sum of squared errors; (ii) *R*-square; (iii) adjusted *R*-square; and (iv) root mean squared error.

The only parameters fixed in the fit were the actual B_1 (Equation 1) and T_1 (set to unity) for all pools except water.

$$B_1(\mathrm{actual}, \mu\mathrm{T}) = B_1(\mathrm{nominal}, \mu\mathrm{T})B_1(\mathrm{relative}). \quad (1)$$

To correct for the effects of the traditional MT and direct water saturation, the amide-CEST effect size (contribution to the *Z*-spectrum) was quantified by the pool difference method using the inverse metrics[34,35]:

$$\mathrm{MTR}_{\mathrm{Rex,amide}}, = \frac{1}{M_z(3.5\mathrm{ppm}, M_\mathrm{b} = 1)/M_0} - \frac{1}{M_z(3.5\mathrm{ppm}, M_\mathrm{b} = 0)/M_0} \quad (2)$$

where $\mathrm{MTR}_{\mathrm{Rex,amide}}$ is the effect size of the cytosolic amides, $M_z(\Delta\omega, M_\mathrm{b})$ is the signal in the *Z*-spectrum at $\Delta\omega$ ($\Delta\omega$ = 3.5 ppm for amide-CEST), M_0 is the equilibrium magnetization at the normalization offset $\Delta\omega$ = 500 ppm and M_b is the amplitude of the amide compartment (M_b = 0 and M_b = 1 for the system without and with amide-CEST pool, respectively). (M_b = 0) − (M_b = 1) gives the amide-CEST pool, hence the name "pool difference method". The pool difference method used in this work was based on the inverse metrics approach and hence the reciprocals in Equation 2.

TABLE 1 The parameters used for fitting the Bloch-McConnell equations to CEST spectra

		Water	Amide-CEST	NOE(Pool 1)	MT	Amine-CEST	NOE*(Pool 2)
T_1 (s)	X_0	1.5	1	1	1	1	1
	LB	1.0	–	–	–	–	–
	UB	2.5	–	–	–	–	–
T_2	X_0	50 ms	10 ms	0.5 ms	20 μs	10 ms	0.5 ms
	LB	20 ms	0.2 ms	0.1 ms	10 μs	0.2 ms	0.1 ms
	UB	70 ms	15 ms	10 ms	80 μs	15 ms	10 ms
Δω(ppm)	X_0	0	3.5	−3.5	−2.4	2.0	−1.6
	LB	−0.1	3.0	−4.0	−4.0	1.5	−1.8
	UB	0.1	4.0	−3.0	−2.0	2.5	−1.4
M_0 (%)	X_0	–	0.1	4.5	9	0.01	1
	LB	–	0	0	0	0	0
	UB	–	0.2	13.5	27	0.10	10
k (Hz)	X_0	–	50	10	50	1 000	10
	LB	–	0	0	0	0	0
	UB	–	600	50	150	10 000	50

X_0, LB and UB represent the initial guess and lower and upper bounds, respectively.

A similar equation applies to the NOE pool ($MTR_{Rex,NOE}$) at Δω = −3.5 ppm. The apparent exchange dependent relaxation (AREX or relaxation compensated MTR_{Rex})[34–37] was not calculated, since the B_1 dependence remains the same for MTR_{Rex} and AREX. The strength of a linear relationship between paired data was determined by the Pearson correlation coefficient (R).

2.4 | Bloch-McConnell equation B_1 correction

The workflow of the Bloch-McConnell equation (BE) B_1 correction algorithm is illustrated in the flowchart (Figure 1). First, the densely sampled Z-spectra are acquired. Second, multi-pool BEs are fitted to the spectra to determine T_1 (spin–lattice relaxation time), T_2 (spin–spin relaxation time), Δω (chemical shift with respect to water), M_0 (pool size), and R_{ex} (exchange rate). The only parameters fixed during the fitting process are B_1(actual), since this parameter is known from a B_1 map used as a reference (Equation 1), and T_1 (fixed to unity) for all pools other than water. Then, the Z-spectra are recalculated at a nominal B_1 level (B_1 = 100%) using the previously fitted BE parameters. Finally, the B_1-corrected effect size of amide and NOE is isolated using Equation 2.

2.5 | Linear model B_1 correction

The first and the second steps of the linear B_1 correction algorithm are identical to those of the BE B_1 correction algorithm (Figure 1). In the

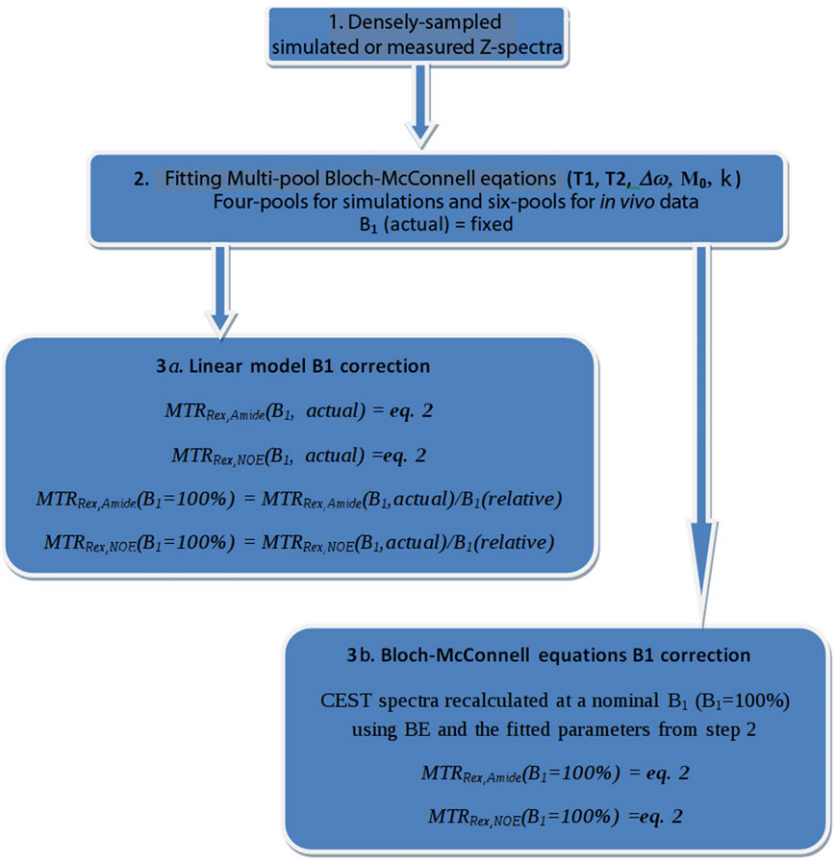

FIGURE 1 A flowchart representing the steps for implementing a linear model and BE B_1 correction algorithms.

third step, the effect size of amide and NOE is isolated using Equation 2 and a linear B_1 correction is achieved by division of the isolated effects by the relative B_1.

2.6 | Comparison with interpolation-based B_1 correction

Both B_1 correction algorithms analyzed in this work were compared with the ideal interpolation-based B_1 correction approach.[23]

The contrast maps of amide and NOE were generated at all B_1 levels as described in the flowchart (Figure 1, Steps 1 and 2) and using Equation 2 to extract the effect sizes. The B_1-corrected maps of both amide and NOE effects were produced by voxel-wise spline interpolation of the corresponding MTR_{Rex} maps at all B_1 levels to a B_1 of 0.43 μT using the eight-point contrast B_1 correction as explained in Reference [23].

3 | RESULTS

3.1 | Numerical simulations

In Figure 2, the BEs were used to simulate the B_1 dependence of amide-CEST ($MTR_{Rex,amide}$) and NOE ($MTR_{Rex,NOE}$) effect size. In the low B_1 regime (0.1–0.5 μT), the B_1 dependence of the effects is largely linear: R = 0.99 (p < 0.005) for both $MTR_{Rex,amide}$ and $MTR_{Rex,NOE}$. There are noticeable rotation effects for $MTR_{Rex,amide}$ at a B_1 above 0.8 μT.[38–40]

The concept of the BE B_1 correction is shown in Figure 3, where a series of Z-spectra was simulated in the B_1 range 0.1–0.5 μT and subsequently fitted using BEs (Figure 3A). The BE fit parameters from Figure 3A were used to recalculate all of the spectra at a B_1 of 0.43 μT (Figure 3B). The overlap of the BE B_1-corrected Z-spectra suggest that BEs may correct the effects of B_1 inhomogeneity. Assuming a nominal B_1 of 0.43 μT, the B_1 range 0.1–0.5 μT used in the simulations (Figure 3A) is expected in the *in vivo* experiments because of B_1 inhomogeneity (typically 60–120%). The effects of amide-CEST ($MTR_{Rex,amide}$) and NOE ($MTR_{Rex,NOE}$) isolated from these Z-spectra

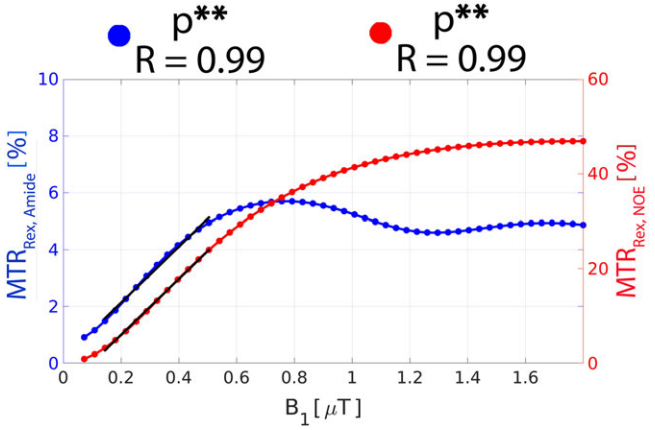

FIGURE 2 The Bloch-McConnell equation simulated B_1 dependence of the effect size of $MTR_{Rex,amide}$ and $MTR_{Rex,NOE}$ in WM. The straight black lines represent the linear regression relation between the corresponding metrics and B_1 in the B_1 range 0.1–0.5 μT. The Pearson correlation coefficient (R) and the corresponding p-value are provided. **Statistical significance at the level p < 0.005.

are termed uncorrected, i.e. without correction for the B_1 inhomogeneity. In Figure 4, the uncorrected effect size of $MTR_{Rex,amide}$ (Figure 4A, blue) and $MTR_{Rex,NOE}$ (Figure 4B, blue) is plotted versus B_1, and compared with those yielded by the linear (red) and the BE B_1 correction (black) algorithms. As expected, both $MTR_{Rex,amide}$ and $MTR_{Rex,NOE}$ uncorrected effects have a strong positive B_1 correlation (R = 0.99 for both effects). The BE B_1 correction over- and underestimated $MTR_{Rex,amide}$ effect size at low and high B_1, respectively (R = −0.88, black), whereas the linear B_1 correction showed a relatively stable effect size across the whole B_1 range simulated (R = 0.09, red). For $MTR_{Rex,NOE}$, the BE B_1 correction also over- and underestimated the effect size at low and high B_1, respectively (R = 0.99, black), whereas the linear B_1 correction reduced the effect of B_1 inhomogeneity (R = 0.95, red). In addition, the BE B_1 correction reversed the sign of the Pearson correlation coefficient due to the over- and under-compensation at low and high B_1, respectively.

3.2 | Experimental results

The experimentally derived B_1 dependence of $MTR_{Rex,amide}$ and $MTR_{Rex,NOE}$ is plotted in Figure 5. As predicted in the simulations (Figure 2), both effects are linear with B_1 in the range 0.1–0.5 μT (R = 0.97 and R = 0.98 for $MTR_{Rex,amide}$ and $MTR_{Rex,NOE}$, respectively), after which the effects start to level off. A nominal B_1 level of 0.43 μT was chosen to compare the performance of the linear model and the BE B_1 correction algorithms, because it is still in the linear B_1 regime and yields a good effect size of both of $MTR_{Rex,amide}$ and $MTR_{Rex,NOE}$. At this power level, the effect size of amide and NOE is reduced by 15% and 10%, respectively, relative to their corresponding maxima. In Figure 6, the correction of transmit field inhomogeneity effects by BEs is demonstrated using the experimental *in vivo* data. The CEST spectra from white matter (Figure 6A) at four power levels, 0.14 μT, 0.29 μT, 0.43 μT, and 0.50 μT, were fitted with BEs (Figure 6B) and subsequently recalculated at a B_1 of 0.43 μT (Figure 6C), resulting in the overlap of BE B_1-corrected spectra.

As expected from the simulations (Figure 2) and the experiments (Figure 5), the visual inspection reveals a strong correlation of uncorrected maps of $MTR_{Rex,amide}$ and $MTR_{Rex,NOE}$ (Figure 7B) with the relative B_1 map (Figure 7A): a high signal in the center and low at the sides. The linear B_1 correction appears to alleviate the issue of B_1 inhomogeneity effectively and create a homogeneous contrast for both $MTR_{Rex,amide}$ and $MTR_{Rex,NOE}$, whereas the BE B_1 correction results in the over- and under-correction of B_1 inhomogeneity effects at low and high power, respectively. Interestingly, both the linear model and the interpolation produced contrast maps of similar quality for both $MTR_{Rex,amide}$ and $MTR_{Rex,NOE}$.

A graphical representation of the contrast distribution is another way to compare the performance of the linear model and the BE B_1-correction approaches. When compared with the uncorrected contrast, the linear B_1 correction effectively reduced the data dispersion (reflected in the box and whiskers above each distribution) for both $MTR_{Rex,amide}$ (Figure 8A,B) and $MTR_{Rex,NOE}$ (Figure 8C,D). Both the linear and the interpolation B_1 corrections seem to produce similar contrast distributions. The BE B_1 correction algorithm clearly over-corrected

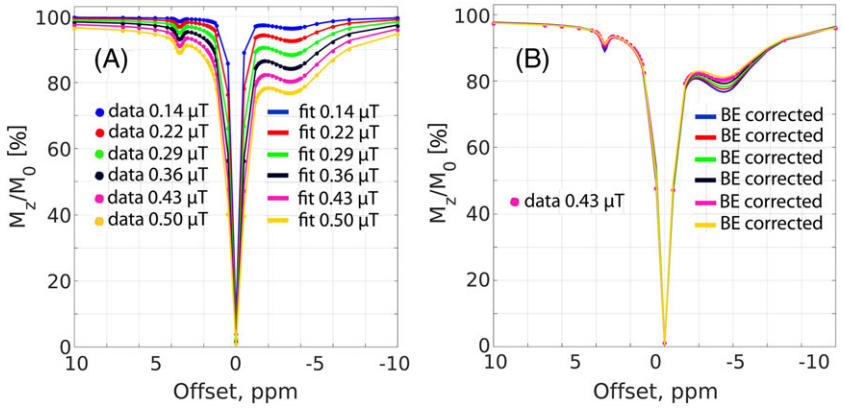

FIGURE 3 A, The four-pool Bloch-McConnell equation simulated spectra (colored markers) at various B_1 levels and their corresponding four-pool Bloch-McConnell fits (colored solid lines). B, Same as A for the colored markers, but the colored solid lines represent BE-corrected spectra recalculated at a B_1 of 0.43 µT (assumed to be nominal B_1 level) using the corresponding fitting parameters from A. A Gaussian noise of 1% (of the signal at 500 ppm) was added to the simulated data.

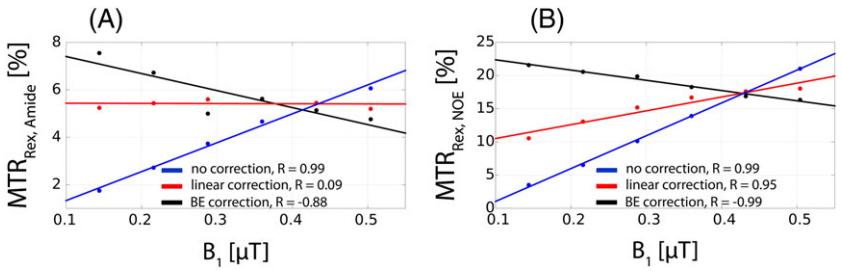

FIGURE 4 A, The comparison of uncorrected (isolated from Figure 3A), the linear model B_1-corrected (isolated from Figure 3A with the subsequent linear B_1 correction), and the BE B_1-corrected (isolated from Figure 3B) $MTR_{Rex,amide}$ effect size as a function of B_1. B, The same as A but for $MTR_{Rex,NOE}$ effect size. For the linear B_1 correction, a B_1 of 0.43 µT was assumed to be nominal B_1 (100%). All other B_1 levels were translated to percentages accordingly. The straight colored lines represent the linear regression relation between the corresponding metrics and B_1. The Pearson correlation coefficient (R) is shown in each subfigure.

data, resulting in a very broad distribution, which can also be seen by visual inspection of the images in Figure 7B.

As expected, a strong correlation of the uncorrected contrast $MTR_{Rex,amide}$ (Figure 9A,B) and $MTR_{Rex,NOE}$ (Figure 9C,D) with B_1 is evident in Figure 9. For example, the correlation coefficient (R) of the uncorrected $MTR_{Rex,amide}$ (Figure 9A) and $MTR_{Rex,NOE}$ (Figure 9C) was found to be 0.65 in WM. The linear B_1 model virtually nullified the correlation by reducing the correlation coefficients to −0.04 (Figure 9A) and 0.01 (Figure 9C) for $MTR_{Rex,amide}$ and $MTR_{Rex,NOE}$, respectively. In line with the simulations in Figure 4 and the experimental results shown in Figure 7B, Figure 8 and Figure 9, the BE B_1 correction algorithm resulted in over- and under-correction at low and high B_1, respectively.

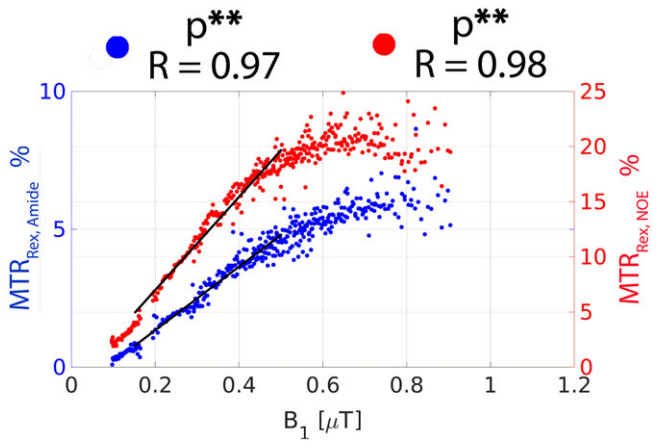

FIGURE 5 The experimentally derived plots of $MTR_{Rex,amide}$ and $MTR_{Rex,NOE}$ as a function of the actual B_1 values in WM. The traces were obtained by segmenting the relative B_1 map (Figure 7A) into the different regions between 50% and 150% in steps of 1% and calculating the corresponding $MTR_{Rex,amide}$ and $MTR_{Rex,NOE}$ contrast resulting from all available CEST datasets. The straight black lines represent the linear regression relation between the corresponding metrics and B_1 in the B_1 range 0.1–0.5 µT. The Pearson correlation coefficient (R) and the corresponding p-value are provided. **Statistical significance at the level $p < 0.005$.

4 | DISCUSSION

In this work, we compared two algorithms for B_1 correction of amide-CEST ($MTR_{Rex,amide}$) and NOE ($MTR_{Rex,NOE}$) effects at 7 T. Both methods rely on fitting the multi-pool BEs to densely sampled CEST spectra to extract the effects. The first algorithm is based on a simple linear model B_1 correction of the isolated effects. The second algorithm uses the fit parameters to recalculate the Z-spectra at a B_1 of interest followed by extraction of the B_1-corrected effects. Both algorithms were compared in the BE simulated and experimental *in vivo* data of the brain of a healthy volunteer. In the BE simulated data, a simple linear model appeared to be more effective in mitigating B_1 inhomogeneity effects. In line with the simulations, the linear B_1 correction outperformed the BE B_1 correction algorithm in the experimental data obtained in the healthy human brain. The linear B_1 correction generated homogeneous image contrast for both $MTR_{Rex,amide}$ and

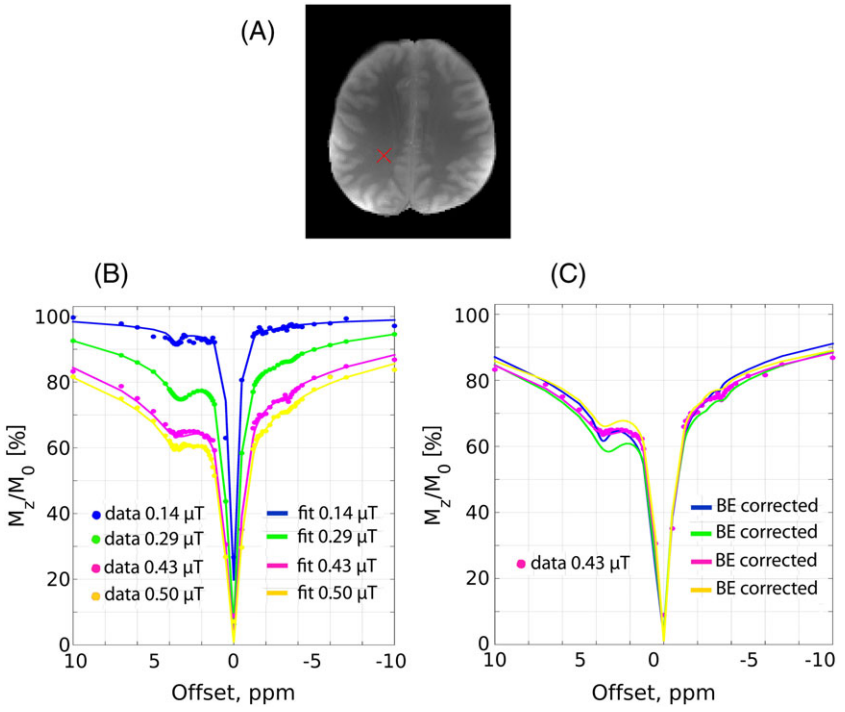

FIGURE 6 A, A CEST image of the healthy human brain with the cross marking the origin of the CEST spectra shown in B and C. B, The *in vivo* CEST spectra (colored markers) at various B_1 levels and their corresponding six-pool Bloch-McConnell fits (colored solid lines). C, Same as B for the colored markers, but the colored solid lines represent BE-corrected spectra recalculated at a B_1 of 0.43 µT (assumed to be nominal B_1 level) using the corresponding fitting parameters from B.

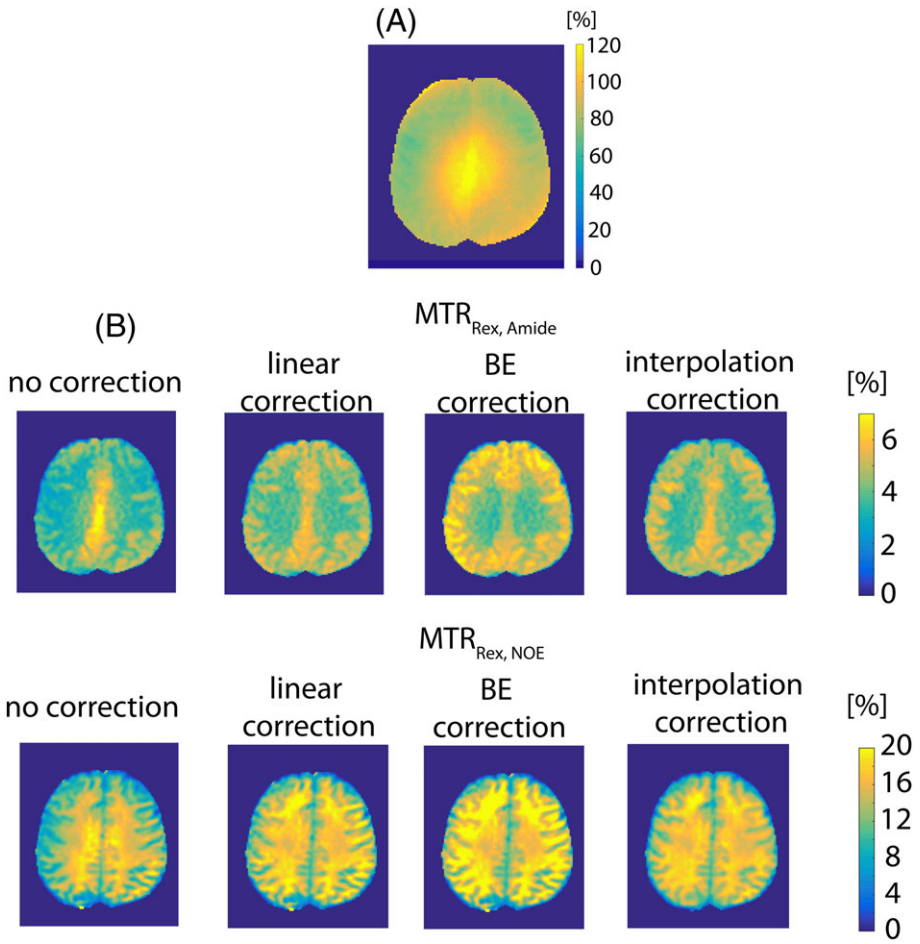

FIGURE 7 A, A relative B_1 map. B, Comparison of the experimentally derived uncorrected, the linear model B_1-corrected, the BE B_1-corrected and the interpolation-based B_1-corrected contrast for $MTR_{Rex,amide}$ (top row) and $MTR_{Rex,NOE}$ (bottom row).

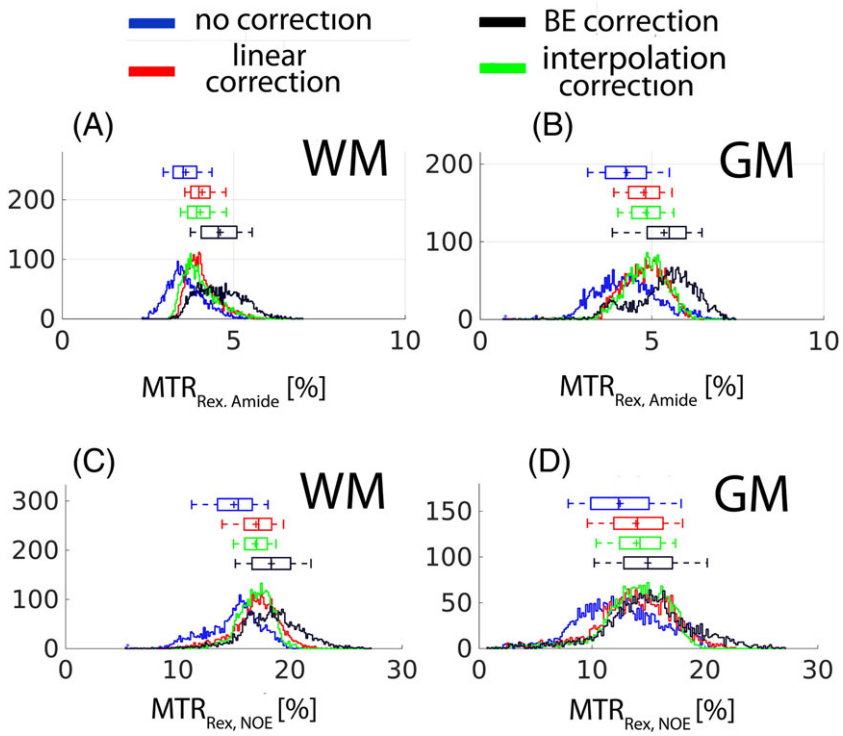

FIGURE 8 The histograms of the images shown in Figure 7B. A,B, WM and GM, respectively, for $MTR_{Rex,amide}$. C,D, WM and GM, respectively, for $MTR_{Rex,NOE}$. The box and whiskers above each histogram contain values of 25–75% and 9–91%, respectively.

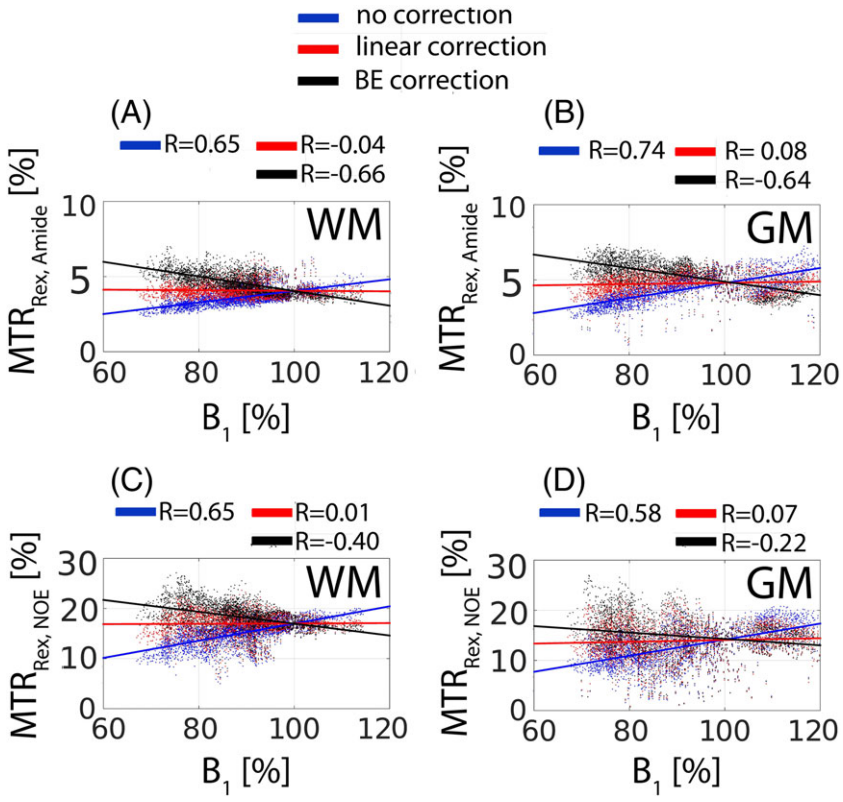

FIGURE 9 The voxel-wise correlation of the image contrast (Figure 7B) with the relative B_1 map (Figure 7A). A,B, WM and GM, respectively, for $MTR_{Rex,amide}$. C,D, WM and GM, respectively, for $MTR_{Rex,NOE}$. The linear colored lines represent the linear regression. The Pearson correlation coefficient (R) is shown in each subfigure.

$MTR_{Rex,NOE}$ and resulted in almost zero correlation of the effects with B_1, whereas the BE B_1 correction algorithm greatly overcompensated the areas with low B_1, thereby increasing the contrast dispersion.

4.1 | Numerical simulations

The four-pool BE simulations suggest a linear B_1 dependence of $MTR_{Rex,amide}$ (R = 0.99, p < 0.005) and $MTR_{Rex,NOE}$ (R = 0.99, p < 0.005) in the low B_1 range 0.1–0.5 μT (Figure 2). This opens up the possibility of a simple linear correction of B_1 inhomogeneity of both effects in this low B_1 regime. The $MTR_{Rex,amide}$ rotation effects[38–40] may pose a challenge when making B_1 corrections at higher B_1 levels.

The perfectly fitted simulated spectra (Figure 3A) and the visual inspection of the overlapping BE B_1-corrected CEST spectra (Figure 3B) suggest that fixing only one B_1 parameter in the BEs and allowing the

rest to vary within reasonable constraints is sufficient to fit and correct the CEST spectra for B_1 inhomogeneity in this low B_1 range, 0.1–0.5 μT. However, care must be taken since the similarity between the BE B_1-corrected spectra does not guarantee that they contain similar CEST features, i.e. $MTR_{Rex,amide}$ and $MTR_{Rex,NOE}$, which are of interest and should be isolated from the spectra. Therefore, for the fair comparison of both B_1 correction algorithms, we chose to compare them in terms of the B_1-corrected $MTR_{Rex,amide}$ and $MTR_{Rex,NOE}$ effects.

The BEs incorporate the effect of chemical exchange and are known to describe the exchange-mediated processes precisely.[24] However, many parameters are correlated, e.g. T_2 and k, k and M_0,[41] which makes it extremely difficult to determine those unambiguously from fitting a single CEST spectrum at one power level. This uncertainty propagates further when recalculating the spectra at a nominal B_1 (B_1 = 100%) and extracting the B_1-corrected contrast, since R_{ex} has an effect on the contrast B_1 sensitivity.[42] The over- and under-correction of $MTR_{Rex,amide}$ and $MTR_{Rex,NOE}$-contrast by the BE B_1 correction algorithm at low and high B_1 levels, respectively (Figure 4A,B, respectively), can be attributed to the parameter correlation. The better performance of the linear B_1 correction can be explained by the absence of an extra step involving the Bloch equation numerical calculations. In addition, a linear relation of $MTR_{Rex,amide}$ and $MTR_{Rex,NOE}$ with B_1 was predicted in the simulations (Figure 2).

The simulation results should be treated with caution, since an assumption was made on the initial pool parameters. In addition, there is no agreement in the literature on the number of pools and the simulation parameters.[26,30–33]

4.2 | Experimental results

Fitting *in vivo* CEST spectra using BEs is a challenge since the exact number of pools is unknown beforehand. In this work, we chose to use six-pool BEs to approximate the *in vivo* complexity. The strong positive linear relationships of $MTR_{Rex,amide}$ (R = 0.97, p < 0.005) and $MTR_{Rex,NOE}$ (R = 0.98, p < 0.005) with B_1 in the range 0.1–0.5 μT (Figure 5) lead us to hypothesize that a simple linear B_1 correction may be sufficient *in vivo* in this B_1 range. The fact that both the simulations (Figure 2) and the experiments (Figure 5) showed a linear relation of $MTR_{Rex,amide}$ and $MTR_{Rex,NOE}$ with B_1 in the low B_1 regime (0.1–0.5 μT) suggests that the simulation parameters chosen in this study were within the acceptable range. The linear correction *in vivo* in this linear B_1 regime comes at the cost of a small reduction in the extracted effect size compared with that obtained at a B_1 level beyond the linear regime. The data dispersion in contrast of $MTR_{Rex,amide}$ and $MTR_{Rex,NOE}$ at high B_1 in Figure 5 may be associated with the presence of labile protons with a range of exchange rates as would be expected *in vivo* as opposed to the constants used in the simulated data. The higher B_1 increases sequence sensitivity to the metabolites bearing labile protons with faster exchange rates. In addition, the results were averaged across small ROIs, which may have different pool parameters. Six pools were sufficient to fit the BEs to the WM (Figure 6A) *in vivo* CEST spectra (Figure 6B) in the low B_1 regime and the overlap of the BE B_1-corrected (recalculated to a nominal B_1 of 0.43 μT) CEST spectra (Figure 6C) suggest that multi-pool BEs may alleviate the issue of transmit field inhomogeneity.

The interpolation B_1 correction method[23] can be considered an ideal B_1 correction approach due to its applicability to any *in vivo* system at any B_1 level. Therefore, all contrast maps generated, uncorrected, linearly and BE B_1 corrected, were compared with those produced by the interpolation (Figure 7B). Only the linearly B_1-corrected maps of both $MTR_{Rex,amide}$ and $MTR_{Rex,NOE}$ effects resemble those generated by the interpolation in terms of the image quality and the effect size, which further validates our assumption of a linear B_1 correction in the low B_1 regime (Figure 8 and Figure 9). For more detailed analysis of the interpolation B_1 correction approach, e.g. number of B_1 levels, image quality, etc., the interested reader is referred to the original work by Windschuh et al.[23] However, the interpolation method always requires multiple acquisitions with varying B_1 levels; a more elegant approach using only a single acquisition would of course be favorable. The authors also compared the interpolation B_1 correction with the linear correction. For the comparison, the authors assumed a linear dependence of CEST effects up to a B_1 of 0.65 μT. However, a linear model is no longer valid at this high power (Figure 5), and so the authors concluded that at least two B_1 levels were necessary for B_1 correction. Yet, we show that a small compromise in the effect size of amide (15%) and NOE (10%), caused by reduced B_1 level to be in the linear regime, leads to a simple B_1 correction method.

The data dispersion and the contrast over- and under-correction by the BE B_1-correction algorithm are clearly noticeable when comparing the interpolation and the BE B_1-corrected maps (Figure 7B), the histogram (Figure 8), and the linear regression analysis (Figure 9). We attribute this to the correlation of the fitted parameters. A total of 22 parameters were fitted to the *in vivo* data and many of the parameters are highly correlated, i.e. have the same effect on CEST spectra appearance. This great number of degrees of freedom, along with the fact that many of the Bloch-McConnell estimated fit parameters are not independent of the actual B_1, may cause an unpredictable system behavior when recalculating CEST spectra at a B_1 of 100% using the non-linear system of BEs to describe a simple linear relationship. The following fit parameters were found to have a significant correlation (R) with B_1: water T_1 (−0.20), water T_2 (0.29), amide T_2 (−0.35), NOE k (−0.22), MT k (−0.37), MT T_2 (−0.31), amine k (−0.19), and NOE* k (−0.20). While the performance of the algorithm may be further improved by measuring and fixing other parameters, e.g. exchange rate and T_2, this would make this method highly inefficient since the clinical scan time is very limited. Fixing water T_1, however, did not improve the performance of the BE B_1-correction algorithm. In this manuscript, the strong linear correlation between M_0 (concentration) and k (exchange rate), which is difficult to decouple,[41] has been exploited to our advantage. For the same effect size (amide or NOE) a low fitted M_0 will be compensated by a high fitted k and vice versa. The B_1 correction algorithms in this work apply to the effect size (a product of M_0 and k), and so the individual parameters are less relevant as long as the BEs fit the original data.

Despite the fact that the linear B_1 correction algorithm was shown only on healthy brain, it is expected to be applicable to pathological tissue as well. Abnormally high water T_1 expected in tumors will scale the CEST effect,[34,35] but the linear B_1 dependence of amide-CEST and NOE effects at low power levels will not change with water T_1 (Supporting Information SI1, Figure S1). The same is true for different CEST saturation parameters, e.g. saturation duration and duty cycle, as

long as the average power, which takes account of the CEST saturation parameters,[43] is low (0.1–0.5 μT). A change in water T_1 and CEST saturation parameters may, however, cause a variation in amide-CEST and NOE signal losses using the linear assumption when compared with measuring the effects at optimal B_1 levels.

In this work, we opted for the use of the multi-pool BE to extract amide and NOE features from CEST data as it is the only approach that intrinsically incorporates the sequence parameters, e.g. B_1 and other CEST saturation prepulse parameters, and the physiological parameters, e.g. metabolite concentration and pH-dependent exchange rate of labile protons with water. Yet, we expect the linear B_1 correction to be applicable to the other methods used for amide and NOE isolation such as the three point method[44], the Lorentzian difference method,[13,45] and multiple Lorentzian fitting[23,46].

5 | LIMITATIONS

The B_1 correction algorithms analyzed in this work are based on the multi-pool Bloch-McConnell equation fitting of densely sampled CEST spectra. An assumption is made as to the number of pools in the system, which is unknown *a priori*. This may require a test fit of the Bloch-McConnell equations to a sample spectrum with an increasing number of pools. To determine the minimum number of pools necessary to describe the *in vivo* system of interest, the fit precision should be monitored by checking the sum of the squares of the residuals or any other appropriate measure.

6 | CONCLUSIONS

In this work, we compared two approaches to the transmit field inhomogeneity correction of the relaxation compensated amide-CEST and NOE effects. Both methods were compared in simulated and *in vivo* brain data obtained in a healthy human volunteer. A simple linear model for B_1 correction outperformed a B_1 correction algorithm based on the Bloch-McConnell equations at the low power levels (0.1–0.5 μT). This was demonstrated by the improved image quality, reduced data dispersion and virtually nullified correlation of the CEST contrast with B_1.

ACKNOWLEDGEMENTS

The financial support of the European Commission under FP7 Marie Curie Actions (FP7-PEOPLE-2012-ITN-316716) is gratefully acknowledged.

REFERENCES

1. Sherry AD, Woods M. Chemical exchange saturation transfer contrast agents for magnetic resonance imaging. *Annu Rev Biomed Eng*. 2008;10:391–411.
2. van Zijl PCM, Yadav NN. Chemical exchange saturation transfer (CEST): what is in a name and what isn't? *Magn Reson Med*. 2011;65(4):927–948.
3. Zaiss M, Bachert P. Chemical exchange saturation transfer (CEST) and MR *Z*-spectroscopy *in vivo*: a review of theoretical approaches and methods. *Phys Med Biol*. 2013;58(22):R221–R269.
4. Vinogradov E, Sherry AD, Lenkinski RE. CEST: from basic principles to applications, challenges and opportunities. *J Magn Reson*. 2013;229:155–172.
5. Cai K, Haris M, Singh A, et al. Magnetic resonance imaging of glutamate. *Nat Med*. 2012;18(2):302–306.
6. Walker-Samuel S, Ramasawmy R, Torrealdea F, et al. *In vivo* imaging of glucose uptake and metabolism in tumors. *Nat Med*. 2013;19(8):1067–1072.
7. van Zijl PC, Jones CK, Ren J, Malloy CR, Sherry AD. MRI detection of glycogen *in vivo* by using chemical exchange saturation transfer imaging (glycoCEST). *Proc Natl Acad Sci U S A*. 2007;104(11):4359–4364.
8. Haris M, Cai K, Singh A, Hariharan H, Reddy R. *In vivo* mapping of brain myo-inositol. *Neuroimage*. 2011;54(3):2079–2085.
9. Ling W, Regatte RR, Navon G, Jerschow A. Assessment of glycosaminoglycan concentration *in vivo* by chemical exchange-dependent saturation transfer (gagCEST). *Proc Natl Acad Sci U S A*. 2008;105(7):2266–2270.
10. Zhou J, Lal B, Wilson DA, Laterra J, van Zijl PC. Amide proton transfer (APT) contrast for imaging of brain tumors. *Magn Reson Med*. 2003;50(6):1120–1126.
11. Jones CK, Schlosser MJ, van Zijl PCM, Pomper MG, Golay X, Zhou J. Amide proton transfer imaging of human brain tumors at 3 T. *Magn Reson Med*. 2006;56(3):585–592.
12. Wen Z, Hu S, Huang F, et al. MR imaging of high-grade brain tumors using endogenous protein and peptide-based contrast. *Neuroimage*. 2010;51(2):616–622.
13. Jones CK, Huang A, Xu J, et al. Nuclear Overhauser enhancement (NOE) imaging in the human brain at 7 T. *Neuroimage*. 2013;77:114–124.
14. Xu X, Yadav NN, Zeng H, et al. Magnetization transfer contrast-suppressed imaging of amide proton transfer and relayed nuclear overhauser enhancement chemical exchange saturation transfer effects in the human brain at 7 T. *Magn Reson Med*. 2016;75(1):88–96.
15. Zhou J, Blakeley JO, Hua J, et al. Practical data acquisition method for human brain tumor amide proton transfer (APT) imaging. *Magn Reson Med*. 2008;60(4):842–849.
16. Togao O, Yoshiura T, Keupp J, et al. Amide proton transfer imaging of adult diffuse gliomas: correlation with histopathological grades. *Neuro Oncol*. 2014;16(3):441–448.
17. Sakata A, Okada T, Yamamoto A, et al. Grading glial tumors with amide proton transfer MR imaging: different analytical approaches. *J Neurooncol*. 2015;122(2):339–348.
18. Dula AN, Arlinghaus LR, Dortch RD, et al. Amide proton transfer imaging of the breast at 3 T: Establishing reproducibility and possible feasibility assessing chemotherapy response. *Magn Reson Med*. 2013;70(1):216–224.
19. Sagiyama K, Mashimo T, Togao O, et al. In vivo chemical exchange saturation transfer imaging allows early detection of a therapeutic response in glioblastoma. *Proc Natl Acad Sci U S A*. 2014;111(12):4542–4547.
20. Zhou J, Tryggestad E, Wen Z, et al. Differentiation between glioma and radiation necrosis using molecular magnetic resonance imaging of endogenous proteins and peptides. *Nat Med*. 2010;17(1):130–134.
21. Paech D, Burth S, Windschuh J, et al. Nuclear Overhauser enhancement imaging of glioblastoma at 7 Tesla: region specific correlation with apparent diffusion coefficient and histology. *PLoS One*. 2015;10(3):e0121220
22. Zhang XY, Xie J, Xu J, Li H, Gore JC, Zu Z. Assessment of membrane fluidity using nuclear Overhauser enhancement mediated magnetization transfer (NOE-mediated MT). In ISMRM 2015, Toronto, Canada. 1747.
23. Windschuh J, Zaiss M, Meissner JEE, et al. Correction of *B*1-inhomogeneities for relaxation-compensated CEST imaging at 7 T. *NMR Biomed*. 2015;28(5):529–537.
24. McConnell HM. Reaction rates by nuclear magnetic resonance. *J Chem Phys*. 1958;28(3):430–431.
25. Woessner DE, Zhang S, Merritt ME, Sherry AD. Numerical solution of the Bloch equations provides insights into the optimum design of PARACEST agents for MRI. *Magn Reson Med*. 2005;53(4):790–799.

26. Mougin O, Clemence M, Peters A, Pitiot A, Gowland P. High-resolution imaging of magnetisation transfer and nuclear Overhauser effect in the human visual cortex at 7 T. *NMR Biomed*. 2013;26(11):1508–1517.
27. Ramani A, Dalton C, Miller DH, Tofts PS, Barker GJ. Precise estimate of fundamental *in-vivo* MT parameters in human brain in clinically feasible times. *J Magn Reson Imaging*. 2002;20(10):721–731.
28. Schmitt B, Zaiß M, Zhou J, Bachert P. Optimization of pulse train presaturation for CEST imaging in clinical scanners. *Magn Reson Med*. 2011;65:1620–1629.
29. Kim M, Gillen J, Landman BA, Zhou J, van Zijl PC. Water saturation shift referencing (WASSR) for chemical exchange saturation transfer (CEST) experiments. *Magn Reson Med*. 2009;61(6):1441–1450.
30. Zhou J, Payen JFF, Wilson DA, Traystman RJ, van Zijl PC. Using the amide proton signals of intracellular proteins and peptides to detect pH effects in MRI. *Nat Med*. 2003;9(8):1085–1090.
31. Liu G, Ali MM, Yoo B, Griswold MA, Tkach JA, Pagel MD. PARACEST MRI with improved temporal resolution. *Magn Reson Med*. 2009;61(2):399–408.
32. Mougin OE, Coxon RC, Pitiot A, Gowland PA. Magnetization transfer phenomenon in the human brain at 7 T. *Neuroimage*. 2010;49(1):272–281.
33. Liu D, Zhou J, Xue R, Zuo Z, An J, Wang DJJ. Quantitative characterization of nuclear overhauser enhancement and amide proton transfer effects in the human brain at 7 tesla. *Magn Reson Med*. 2013;70(4):1070–1081.
34. Zaiss M, Xu J, Goerke S, et al. Inverse *Z*-spectrum analysis for spill-over-, MT-, and T_1-corrected steady-state pulsed CEST-MRI—application to pH-weighted MRI of acute stroke. *NMR Biomed*. 2014;27(3):240–252.
35. Zaiss M, Windschuh J, Paech D, et al. Relaxation-compensated CEST-MRI of the human brain at 7 T: unbiased insight into NOE and amide signal changes in human glioblastoma. *Neuroimage*. 2015;112:180–188.
36. Khlebnikov V, Polders D, Hendrikse J, et al. Amide proton transfer (APT) imaging of brain tumors at 7 T: the role of tissue water T_1-relaxation properties. *Magn Reson Med*. 2016. doi: 10.1002/mrm.26232
37. Khlebnikov V, Siero JC, Wijnen J, et al. Is there any difference in amide and NOE CEST effects between white and gray matter at 7 T? *J Magn Reson*. 2016;272:82–86.
38. Zu Z, Li K, Janve VA, Does MD, Gochberg DF. Optimizing pulsed-chemical exchange saturation transfer imaging sequences. *Magn Reson Med*. 2011;66(4):1100–1108.
39. Zu Z, Janve VA, Li K, Does MD, Gore JC, Gochberg DF. Multi-angle ratiometric approach to measure chemical exchange in amide proton transfer imaging. *Magn Reson Med*. 2012;68(3):711–719.
40. Zu Z, Janve VA, Xu J, Does MD, Gore JC, Gochberg DF. A new method for detecting exchanging amide protons using chemical exchange rotation transfer. *Magn Reson Med*. 2013;69(3):637–647.
41. Desmond KL, Stanisz GJ. Understanding quantitative pulsed CEST in the presence of MT. *Magn Reson Med*. 2012;67(4):979–990.
42. Xu J, Yadav NN, Bar-Shir A, et al. Variable delay multi-pulse train for fast chemical exchange saturation transfer and relayed-nuclear overhauser enhancement MRI. *Magn Reson Med*. 2014;71(5):1798–1812.
43. Zu Z, Li K, Janve VA, Does MD, Gochberg DF. Optimizing pulsed-chemical exchange saturation transfer imaging sequences. *Magn Reson Med*. 2011;66(4):1100–1108.
44. Jin T, Wang P, Zong X, Kim SG. MR imaging of the amide-proton transfer effect and the pH-insensitive nuclear overhauser effect at 9.4 T. *Magn Reson Med*. 2013;69(3):760–770.
45. Jones CK, Polders D, Hua J, et al. In vivo three-dimensional whole-brain pulsed steady-state chemical exchange saturation transfer at 7 T. *Magn Reson Med*. 2012;67(6):1579–1589.
46. Desmond KL, Moosvi F, Stanisz GJ. Mapping of amide, amine, and aliphatic peaks in the CEST spectra of murine xenografts at 7 T. *Magn Reson Med*. 2014;71:1841–1853.

SUPPORTING INFORMATION

Additional Supporting Information may be found online in the supporting information tab for this article.

How to cite this article: Khlebnikov V, Windschuh J, Siero JCW, et al. On the transmit field inhomogeneity correction of relaxation-compensated amide and NOE CEST effects at 7 T. *NMR in Biomedicine*. 2017;30:e3687. https://doi.org/10.1002/nbm.3687